Ambipolar and Unipolar PbSe Nanowire Field-Effect Transistors

David K. Kim,[†] Tarun R. Vemulkar,[†] Soong Ju Oh,[†] Weon-Kyu Koh,[‡] Christopher B. Murray,[†,‡] and Cherie R. Kagan[†,‡,§,*]

[†]Department of Materials Science & Engineering, [‡]Department of Chemistry, and [§]Department of Electrical Systems and Engineering, University of Pennsylvania, Philadelphia, Pennsylvania 19104, United States

Colloidal semiconductor nanostructures have motivated widespread interest in exploring the fundamental chemical and physical origins that give rise to their unique electrical and optical properties and in harnessing these properties in a range of device technologies, such as low-cost and high performance field effect devices,[1,2] thermoelectrics,[3,4] energy efficient photovoltaics,[5,6] and photodetectors.[7] Of particular interest are nanostructures of lead selenide (PbSe), a high mobility, infrared absorbing semiconductor that exhibits strong quantum confinement in nanostructured materials due to its large Bohr exciton radius ($a_{ex} \approx 46$ nm) and its uniquely large and similar electron and hole Bohr radii ($a_e \approx a_h \approx 23$ nm).[8] Probing the electronic properties of nanostructured materials and exploiting their characteristics in applications require their integration in device architectures. Here we unmask the intrinsic electronic properties of wet-chemically synthesized, PbSe nanowires (NWs) through air-free preparation and integration to form the active, semiconducting channels of field-effect transistors (FETs). We use spatially selective and concentration dependent surface modification to engineer the electrical characteristics of PbSe NW FETs. Ambipolar FETs were prepared at low concentrations of dopants, whereas, at high concentrations, unipolar n- and p-type FETs were formed using hydrazine and oxygen, respectively.

Similar to dopants in bulk semiconductors, exposing the surface of nanocrystals (NCs) to organic compounds has been reported to provide a route to modify the electronic properties of nanostructured materials.[1,9] Most effectively hydrazine has been reported to n-dope PbSe NC and NW FETs[1,10–12] and improve device characteristics[13] at typical hydrazine concentrations of 1 M.[1,10–12,14,15] Removal of hydrazine

ABSTRACT Wet-chemical methods, under rigorous air-free conditions, were used to synthesize single-crystalline 10 nm diameter PbSe nanowires (NWs), and electric-field, directed assembly was employed to align NW arrays to form the semiconducting channels of field-effect transistors (FETs). Electrical measurements revealed as-aligned NWs in bottom, gold, contact FETs are predominantly p-type ambipolar, consistent with the presentation of small barriers to electron and hole injection for this low band gap semiconductor. Exposing the NW FET to UV-ozone p-doped the NWs, illustrating the sensitivity of PbSe to oxygen, but controlled oxidation allowed the fabrication of unipolar p-type FETs. Selectively exposing the contact region of as-aligned NW FETs to low to moderate concentrations of hydrazine, commonly used to n-dope nanocrystal and NW devices, switched the predominantly p- to n-type ambipolar behavior as if the entire NW channel was exposed. At these hydrazine concentrations, charge transfer doping the metal—semiconductor interface dominates the FET characteristics. Only upon exposing the NW FETs to high hydrazine concentrations did charge transfer doping of the NW channel overcome the large intrinsic, thermally generated carrier concentration of this low band gap material, modulating the NW carrier concentration and forming unipolar n-type FETs. Pulling low vacuum removed surface hydrazine returning the predominantly p-type ambipolar FET behavior. Doping and dedoping with hydrazine were repeatedly reversible. By applying surface modification to n- and p-dope PbSe NW FETs, we fabricated the first PbSe NW inverters, demonstrating the promise of these nanostructured materials in integrated circuits.

KEYWORDS: nanocrystals · colloidal nanowires · electric-field directed assembly · transistors · inverters

returns the NC FET behavior to p-type.[1] Other simple amines[10] and ethanedithiol[14] have also been used to modify nanostructures, but the origin of the observed changes in carrier transport measured in FETs upon ligand exchange is not well understood and remains difficult to control.[11]

Charge transport in NC FETs is further complicated by variations in interparticle spacing and film cracking, as it shrinks upon exchange of the long, insulating ligands used in NC synthesis and assembly with the shorter ligands used to chemically dope and convert the initially insulating film to become conductive. In order to simplify the problem and gain an understanding of the role surface modification has on the electronic properties of nanostructured materials

and their devices, we investigated single-crystalline colloidal nanowires (NWs). The NWs bridge the entirety of the FET channel, avoiding the changes in interparticle spacing and cracking in NC films upon ligand exchange, providing a model system to investigate the role of surface modification on the electrical properties of nanocrystalline PbSe devices. Here, we show, at low concentrations of surface modifiers commonly used to dope NC and NW FETs, charge transfer at the metal−PbSe junction of the FET modifies carrier injection and dominates the measured changes in device behavior. While NCs have a higher surface area and may be more readily doped than NWs, carrier concentration modulation of the NWs in the channel is only observed at much higher concentrations of chemical dopants.

Single-crystalline PbSe NWs were synthesized by wet-chemical methods *via* oriented attachment of NCs, as reported previously.[16] Transmission electron microscopy (TEM) [Figure S1A] shows the synthesis produced single-crystalline PbSe NW samples approximately 10 nm in diameter and over 10 μm in length. Rigorous air-free conditions were used from synthesis to purification, fabrication, and characterization to prevent oxidation of the NWs, which has been observed in PbSe nanostructures.[10,14,17−19] NW solutions were dropcast under dc electric fields of 10^4 to 10^5 V/ cm [Figure S1B], aligning NW arrays across the prefabricated bottom electrodes [Figure S1C, D]. Devices were then well-washed in both ethanol and chloroform to remove excess ligands, namely the oleic acid used in NW synthesis and the hexadecane-graft-polyvinylprrolidone (HD-PVP) used to aid NW dispersion. Transmission FTIR and FET electrical characteristics were correlated with device washing (Figure S2). Removing surface-bound ligands improved FET transport characteristics, whereas insufficient washing led to very poor FET current modulation.

As-aligned PbSe NW FETs show evidence of both hole and electron transport, known as ambipolar transport, but stronger hole transport gives predominantly *p*-type behavior [Figures 1A and S3A, B]. This is observed as the $I_D−V_{DS}$ characteristics show holes accumulate in the NW channel near the source electrode at negative V_{DS} and V_G. The closely spaced, sigmoidal $I_D−V_{DS}$ characteristics at low voltages, known as "current crowding"[20] [highlighted in the inset Figure 1A], limit the device on-current. After multiple washings with ethanol, chloroform, and acetonitrile, the observed "current crowding" remains. We hypothesize that either intervening material or physical space remains between the surface of the electrodes and the NWs, which is not removed upon washings with common solvents. Immersing these devices in 4 M hydrazine in acetonitrile (CH_3CN) for 24 h converts the device behavior to predominantly *n*-type. The device remains ambipolar, as both hole and electron transport are observed, but now the electron transport is more
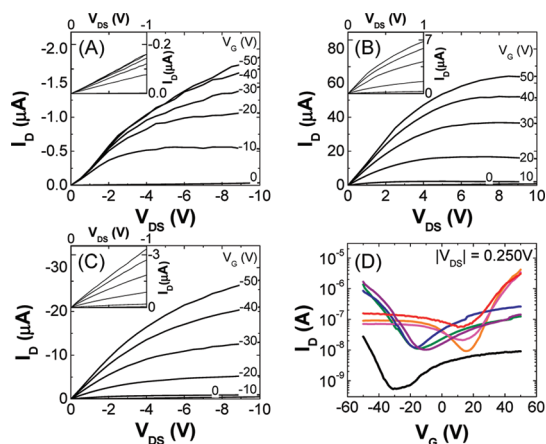

Figure 1. $I_D−V_{DS}$ characteristics of PbSe NW FETs (A) as-aligned, after (B) first immersion in 4 M hydrazine in acetonitrile, and (C) pulling low vacuum. (D) $I_D−V_G$ characteristics of the NW FETs following the reversible conversion of FET behavior from predominantly hole to electron transport corresponding to (black) Figure 1A, (orange) Figure 1B, (green) Figure 1C, (pink) 2nd 4 M hydrazine immersion, (blue) 2nd pulling vacuum, (red) 3rd 4 M hydrazine immersion, and (purple) 3rd pulling vacuum.

significant [Figures 1B and S3C, D]. After hydrazine treatment, the $I_D−V_{DS}$ characteristics are linear at low voltages [inset Figure 1B] and the device on-current I_D is increased by a factor of 40. The electrons accumulate in the NW channel near the source electrode at positive V_{DS} and V_G. Pulling low vacuum (30 mTorr) for an hour on the devices is consistent with removing the hydrazine and recovers the NW FETs' predominantly *p*-type characteristics [Figure 1C]. In order to verify that all of the hydrazine was removed, devices were also placed under high vacuum (10^{-8} Torr) overnight and showed no difference in their characteristics from those pumped under low vacuum. The predominantly *p*-type devices show improved $I_D−V_{DS}$ characteristics [inset Figure 1C] and increased on-current by a factor of 15 compared to as-aligned PbSe NW FETs. Hydrazine, even though it is subsequently removed, is an aggressive and reducing solvent which may make a more intimate metal−NW interface than that of the as-aligned device. We show that this process is repeatedly reversible as NW FETs can be converted from ambipolar, predominantly *p*- to *n*-type, retaining their high current levels, and back over multiple exposures to 4 M hydrazine and removal under vacuum [Figure 1D]. As shown in FTIR spectra [Figure S2], hydrazine does not continue to remove significant quantities of surface-bound oleic acid and HD-PVP but may, as has been proposed, act as a Lewis base[1] or hydrazinium cation at the PbSe NW surface, described further below. In addition to the as-aligned device, all subsequent device characteristics show consistent and reproducible $I_D−V_G$ characteristics, forming ambipolar, predominantly *n*-type FETs upon exposure to hydrazine and predominantly *p*-type FETs with vacuum removal of hydrazine, as exemplified by electron and hole on-currents

[Figure S3E]. The devices retain the same threshold voltage (V_T) for electrons and holes when predominantly n- and p-type, respectively [Figure S3F]. Mobility values for the FETs range from 1 to 10 cm^2/V·s but are based on the lithographically defined channel widths. Based on SEM images, the NWs sparsely span the junction along its 200 μm width (covering approximately 5% of the channel width); the mobility values should be considered a conservative estimate. The reversibility in the NW FET characteristics has been measured over tens of device structures fabricated at different times on different wafers [Figure S3E, F].

While previous work on as-aligned PbSe NW FETs showed only hole transport,[12] rigorous air-free conditions enable these predominantly p-type devices to also show evidence of electron transport, as seen in the I_D–V_G curves [Figure 1D] and the I_D–V_{DS} characteristics in the electron accumulation regime [Figure S3B], indicating ambipolar behavior. The I_D–V_{DS} characteristics of ambipolar FETs show at high negative V_G hole accumulation, at high positive V_G electron accumulation, and at moderate V_G and high negative and high positive V_{DS} both electron and hole accumulation in the FET channel. Even after hydrazine treatment, the devices display ambipolar behavior when either predominantly p- or n-type. The asymmetry in the on-currents (I_{ON}) for both electrons and holes is only about 1 order of magnitude when operating both predominantly p- and n-type devices [Figure S3E], even after multiple cycles of hydrazine exposure and removal. Measurement of the NW absorption in the FTIR reveals these 10 nm diameter NWs have a small effective band gap of 0.45 eV [Figure 2A]. Given the small effective band gap of the NWs, small barriers are presented for both hole and electron injection, as the sum of the energy barriers for electron and hole injection equal that of the energy gap.[20] Given the similar electron and hole mobilities for PbSe, the observed ambipolar behavior at low doping is anticipated. The small band gap of PbSe also manifests in a large population of thermally generated carriers at room temperature, giving rise to off-currents in the range of 1 to 10 nA for thousands of NWs spanning FET channels. By decreasing the operating temperature of the PbSe FET, strong ambipolar behavior is observed with a dramatic increase in the on/off ratio to 10^6 and an increase in both electron and hole mobilities by an order of magnitude [Figure 2B].

The intrinsic ambipolar behavior can easily be missed if rigorous air-free conditions are not used to avoid oxidation of the PbSe nanostructures. Oxygen creates acceptor states in PbSe NCs,[21,22] which cause the material to become strongly p-type, increasing its hole concentration at the expense of its electron concentration and giving rise to a loss of gate modulation[10,14] in FET devices. PbSe NWs also suffer from the same sensitivity to oxygen as bulk PbSe,
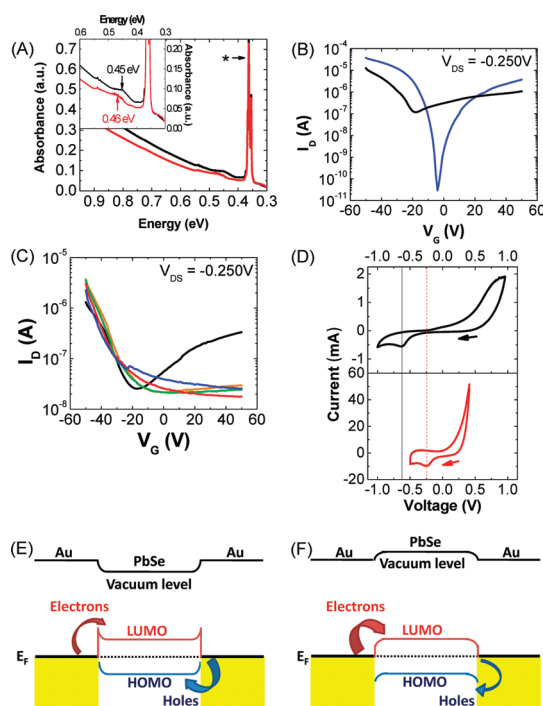

Figure 2. (A) Absorption spectrum of dropcast NWs (black) before oxidation and (red) after 10 min of exposure to UV-ozone (* is from —CH stretches). (B) I_D–V_G characteristics of PbSe NW FETs (black) at room temperature and (blue) 77 K. (C) Room temperature I_D–V_G characteristics of PbSe NW FETs (black) treated with UV-ozone for (orange) 5 s, (green) 10 s, (red) 30 s, and (blue) 60 s. (D) Cyclic voltammetry of PbSe NWs (black) washed in ethanol and (red) subsequently treated in hydrazine. Schematic band diagrams depicting the HOMO, LUMO, and vacuum levels and the Fermi energy (E_F) for (E) as-aligned and (F) 4 M hydrazine treated PbSe NW FETs.

which was verified by a blue shift in the NW absorption peak after a 10 min UV-ozone exposure [Figure 2A]. However, controlled oxygen doping of PbSe FETs may serve to be advantageous for enhanced p-type characteristics. In order to better understand the role of oxygen, devices were treated under UV-ozone for varying times. Starting with an ambipolar p-type PbSe NW FET, we see a significant loss in electron current and a shift in the threshold voltage to more positive voltages even after a short 5 s UV-ozone exposure [Figure 2C], highlighting the importance of air-free conditions in observing the intrinsic PbSe NW character. We see further improvement in the p-type characteristics for UV-ozone treatments up to 10 s, but subsequent UV-ozone treatments longer than 10 s cause the predominantly p-type PbSe NW FET to degrade in performance and to suffer poor gate modulation, similar to the degradation reported for PbS NCs in solar cells.[5] Gold also forms a thin oxide upon exposure to UV-ozone, which acts to increase the metal work function by up to 0.16 eV at room temperature[23] and favors hole injection. However, we observed the electron transport can be recovered after reimmersing the devices in a 4 M hydrazine solution overnight. Gold
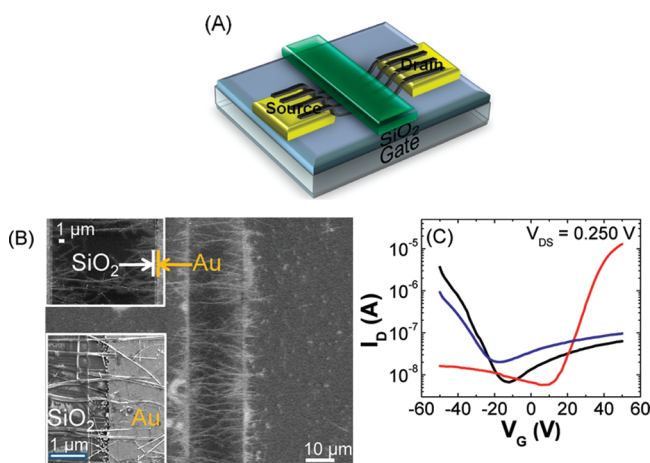
Figure 3. (A) Schematic of PbSe NW FET with top insulating SiO$_2$ blocking layer. (B) SEM of blocking layer atop the PbSe NW FET; (inset) higher resolution images. (C) I_D–V_G characteristics following the conversion of the NW transport behavior when only modifying the NW-metal junction corresponding to the FET upon (black) fabricating the blocking layer, (red) immersing in 4 M hydrazine, and (blue) pulling vacuum.

oxide is unstable in solvent and will be removed,[24] and the NW surface is expected to be reduced by hydrazine.[1] By controlling the UV-ozone exposure time of the NW FET, it is possible to control the degree of *p*-type behavior seen in PbSe FETs, ranging from predominantly *p*-type ambipolar to unipolar *p*-type.

Both optical [Figure 2A] and cyclic voltammetry measurements [Figure 2D] were used to characterize the absolute energy levels of the PbSe NWs before and after hydrazine treatment. The potential was recorded against the oxidation peak of a ferrocene/ferrocenium (Fc/Fc$^+$) redox couple, which has a reported highest occupied molecular orbital (HOMO) energy level of −4.80 eV and served as an external standard in our system.[25] The first reduction peak was used to calculate the lowest unoccupied molecular orbital (LUMO) level, while the HOMO was evaluated using the optical energy gap from FTIR absorption spectroscopy (0.45 eV). Differences in the absolute potential levels of the PbSe NWs are in reference to the Pt electrode, which mimics the change that is observed against Au contacts. Based on the reduction peak for untreated NWs at −0.63 V and hydrazine treated NWs at −0.24 V, we can estimate LUMO/HOMO levels for untreated and hydrazine treated NWs to be 4.17/4.62 eV and 4.56/5.01 eV, respectively. While gold has been reported to have a work function of around 5.1 eV, this energy level can only be attributed to high purity clean gold under ultrahigh vacuum (UHV). Outside of vacuum, the surface of gold is readily contaminated, which can significantly modify its work function to 4.7 eV.[26,27] Since the NWs were dropcast in a nitrogen glovebox rather than in UHV, we expect the gold electrodes to be dirty. Based on the more favorable band alignment of the untreated PbSe HOMO level (4.62 eV) with the work function of the dirty gold contact, the predominantly *p*-type behavior of the as-aligned NW FETs may be attributed to band bending promoting hole injection [Figure 2E]. The

predominantly *n*-type behavior of PbSe NW FETs upon exposure to hydrazine can be attributed to electron transfer from hydrazine to the NW to form N$_2$H$_4^+$,[28−30] which induces a negative charge and forms an inward-pointing surface dipole. This surface dipole reduces the local metal work function and effectively increases the electron affinity and ionization potential of the HOMO and LUMO levels of PbSe nanostructures,[15,31] shifting the material's LUMO level (4.77 eV) to be more favorable toward electron injection [Figure 2F]. This process is reversible in PbSe nanostructures, and once the sample is under vacuum for a period of time, the hydrazine is removed and the work function returns to favor hole injection and suppress electron injection.

To further understand and isolate the role of the metal/semiconductor junction on the measured electrical properties of NW FETs, a SiO$_2$ blocking layer was fabricated on top of 19 μm of the 20 μm NW channel to selectively dope 0.5 μm of the NW at the NW−source and drain interfaces [Figure 3A, B]. All methods to fabricate the blocking layer were carried out in air-free conditions, as rigorously as possible. In fabricating the SiO$_2$ blocking layer, experiments were performed at each processing step, through lithography and SiO$_2$ evaporation, to ensure the integrity of the NW FETs remained unaffected [Figure S4]. There were no signs of NW sintering or growth, as verified by scanning electron microscopy, which is consistent with reported heat treatments of PbSe NC films that show electrical characteristics and conductivity that remain essentially unchanged from the as-made films when heated to 200 °C for 1 h.[10] The e-beam resist developer MIBK:IPA suppressed the device's electron current [Figure S4B], but pulling high vacuum (10^{-8} Torr) on the sample recovered the ambipolar behavior, as shown by the I_D–V_G curve after SiO$_2$ evaporation.

The predominantly *p*-type, ambipolar FET behavior remained intact after fabrication of the blocking layer

[Figure 3C]. Immersing the device in 4 M hydrazine in acetonitrile for 24 h still converted the device to predominantly *n*-type characteristics. Upon removing the hydrazine under vacuum, the device regained its predominantly *p*-type behavior. For predominantly *n*- and *p*-type FETs, the current levels are similar to those for NW FETs without the blocking layer, upon exposure and removal of hydrazine, and show reversible transport behavior by modifying only the contact region. Different blocking layer lengths of 18 and 16 μm were also fabricated on top of the 20 μm channel, creating 1 and 2 μm gaps at the source and drain contact regions. The device current levels for the FETs when exposed to hydrazine and when hydrazine is removed are invariant with the size of the gap at the electrodes, despite the exposure and removal of more of the NW length to hydrazine. Polarity switching of the majority carrier in FETs from hole to electron transport (from *p*-type to *n*-type) by selectively exposing the NW−metal junction and the changes in HOMO and LUMO energies extracted from cyclic voltammetry measurements show that the energy level alignment at the metal−nanostructure contact governs the measured device behavior.

Using 4 M hydrazine, we were unable to achieve completely *n*-type unipolar devices. Therefore PbSe NW FETs were immersed in higher concentrations of hydrazine in acetonitrile [Figure 4A] to see if the devices could be more strongly *n*-doped. Without a blocking layer present, immersing the device in 8 M hydrazine completely turned off the ambipolar behavior and converted the FET to fully *n*-type, shifting V_T to be more negative. By controlling the hydrazine concentration used to charge transfer dope the NW FETs, it is possible to control the degree of electron transport seen in the device, ranging from ambipolar, predominantly *n*-type to unipolar *n*-type behavior. On the other hand, using an SiO_2 blocking layer to protect the NW channel and exposing only the contacts to 8 M hydrazine [Figure 4B], the device characteristics were still ambipolar, predominantly *n*-type. These results show that only modifying the band level alignment at the PbSe−metal junction is not sufficient to make a unipolar device. Since PbSe is a small band gap material, simply shifting the interface dipole without changing the material's intrinsic carrier concentration is not enough to suppress its inherent ambipolar characteristics because PbSe NW FETs will always have small barriers to both electron and hole injection. The only way to fabricate a unipolar device is to change the bulk carrier concentration by increasing the electron concentration at the expense of the hole concentration, similar to our fabrication of unipolar *p*-type devices using oxygen exposure [Figure 2C]. The PbSe FET without a blocking layer upon exposure to 4 M hydrazine still exhibits ambipolar behavior. At low to moderate doping densities, contact modification dominates
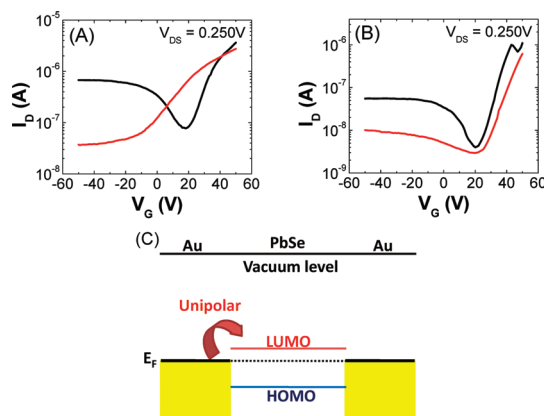

Figure 4. $I_D−V_G$ characteristics of PbSe NW FETs treated with (black) 4 M and (red) 8 M hydrazine, (A) without and (B) with a blocking layer. (C) Schematic band diagram depicting the HOMO, LUMO, and vacuum levels and the Fermi energy (E_F) for 8 M hydrazine doped PbSe NW FETs. Note the influence of 8 M hydrazine on the magnitudes of the doping levels and interface dipole is not known quantitatively.

the measured transport characteristics and the bulk carrier concentration has not been significantly affected. Given that PbSe has a high population of thermally generated carriers, it is necessary to dope at high concentrations (above the level achieved with 4 M hydrazine) to significantly impact the intrinsic carrier density and achieve unipolar transport. Figure 4C shows a schematic band diagram for PbSe NW FETs modified with 8 M hydrazine. Both devices with and without blocking layers treated in 8 M hydrazine can be returned back to their predominantly *p*-type state under low vacuum for 1 h. Immersing the device in 12 M hydrazine ruined the devices, since hydrazine is a caustic base and has been shown to dissolve lead chalcogenides at high concentrations.[32,33]

By taking advantage of the control we have over the PbSe device behavior, we fabricated bottom-contact inverters using a unipolar *p*-type FET (treated for 10 s with UV-ozone) and a unipolar *n*-type FET (treated with 8 M hydrazine) [Figure 5A, B]. The gates of the FETs were connected and used as the input of the inverter. These are the first reported PbSe NW inverters which exhibit promising gains of ∼8 for both positive and negative V_{DD}.

In summary, we report surface treated, bottom-contact PbSe FETs with controllable and reversible device characteristics (V_T, I_{ON}), ranging from oxygen treated unipolar *p*-type, ambipolar to high hydrazine concentration treated unipolar *n*-type. Selectively treating the contacts reversibly changes the predominant measured carrier to holes or electrons, exhibiting the dominating role the metal−semiconductor NW contacts have on charge injection in these devices at low to moderate doping concentrations. The changes in band alignment are also consistent with cyclic voltammetry measurements and reflect the importance of interfacial doping on charge injection in FETs
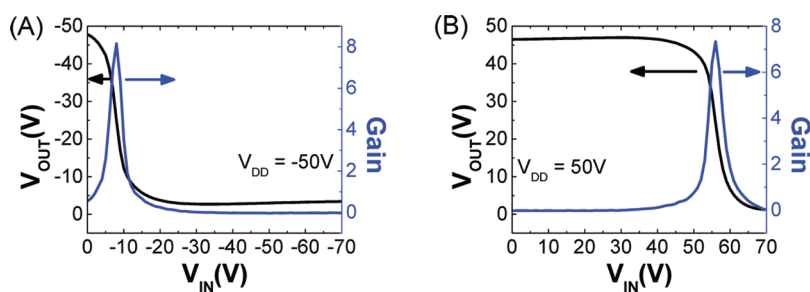
Figure 5. Transfer and gain characteristics of inverters constructed from unipolar *p*- and *n*-type PbSe NW FETs at (A) negative and (B) positive V_{DD}.

for nanostructured materials. Since PbSe is a small band gap semiconductor with a small barrier for both electrons and holes, the device's ambipolar characteristics can only be suppressed by modifying the high concentration of thermally generated carriers at high doping concentrations. Measurements of PbSe nanowire FETs to liquid helium temperatures are being explored to characterize charge injection and transport for different surface modifications and concentrations. By taking advantage of the control we have over electronic properties in PbSe NW FETs, we fabricated the first PbSe NW inverters that show amplification and the promise of these nanostructured materials in integrated circuits. The fabrication processes we developed for the blocking layer successfully preserved the intrinsic properties of these very oxygen and water-sensitive nanomaterials, and we believe it can be used for a variety of other air-sensitive materials and more complicated devices, such as top gate and other dual gate configurations.

METHODS SECTION

Materials for Nanowire Synthesis. All manipulations were carried out using standard Schlenk-line techniques under dry nitrogen. Tri-*n*-octylphosphine (further referred to as TOP, Aldrich, 90%), oleic acid (OA, Aldrich, 90%), diphenyl ether (Aldrich, 99%), amorphous selenium pellets (Aldrich, 99.999%), lead acetate trihydrate (Fisher Scientific Co.), and *n*-tetradecylphosphonic acid (TDPA, Strem, 97%) were used as purchased without further purification. Anhydrous chloroform and hexane were bought from Aldrich. To prepare a 0.167 M stock solution of trioctylphosphine selenide (TOPSe), 1.32 g of selenium was dissolved in 100 mL of TOP overnight by stirring.

Synthesis. The synthesis is based on a previous report:[18] Lead acetate trihydrate (0.76 g) was dissolved in 2 mL of OA and 10 mL of diphenyl ether. The solution was heated to 150 °C for 30 min under nitrogen flow in order to form a lead−oleate complex. The solution was then cooled to 60 °C, and 4 mL of 0.167 M TOPSe solution were added slowly to prevent premature nucleation of PbSe. The combined lead−oleate/TOPSe solution was injected under vigorous stirring into a hot (250 °C) growth solution containing 0.2 g of TDPA dissolved in 15 mL of diphenyl ether. After ∼50 s of heating, the reaction mixture was cooled to room temperature using a water bath. Once cooled, the reaction vessel (still under N_2) was transferred to a glovebox, where the crude solution was mixed with equal amounts of hexane, and the nanowires (NWs) were isolated by centrifugation at 4300 rpm for 5 min. The resulting NW precipitate was redispersed in chloroform for further characterization. Optical absorption spectra of PbSe NWs deposited on double-side polished silicon substrates were collected with a Nicolet 8700 FTIR in transmission. Figure 2A shows the absorption spectra of PbSe NWs.

Device Preparation. Devices were fabricated on an *n*-doped Si wafer with 250 nm thermally grown SiO_2 from Silicon Inc. Electrodes were patterned using photolithography with a bilayer of Lift-off Resist (LOR3A from MicroChem) and S1813 (Microposit). Samples were photolithographically patterned to define channel lengths of 20 μm and widths of 200 μm using a Karl Suss Mask aligner and developed in MF-319 (Microposit). The exposed sample was cleaned by a 3 min O_2 plasma, and metal was deposited by e-beam evaporation of 2 nm of Ti and 18 nm of Au. Metal was subsequently lifted off using Remover

PG (MicroChem). The fabricated devices were then put in a YES (Yield Engineering Systems) Oven, where the fabricated devices were first cleaned with an O_2 plasma and then vapor primed with hexamethyldisilazane (HMDS, Aldrich, 99.9%) for 5 min at 150 °C.

Nanowire Alignment. NWs were dispersed in octane/nonane at a 1:1 (vol:vol) ratio with several drops of 10 wt % solution hexadecane-graft-polyvinylprrolidone (HD-PVP) copolymer ($M_n = \sim$7300) to improve the NWs' dispersibility. NWs were aligned across the device structure having a channel length of 20 μm and channel width of 200 μm. The NWs were washed with ethanol and then chloroform to remove the HD-PVP polymer and organics, which was verified using a Nicolet 6700 FTIR. For *n*-type conversion of the *p*-type NW FETs, varying concentrations of hydrazine (Aldrich, 98%) in acetonitrile (Aldrich, anhydrous, 99.8%) were used. **(NOTE: hydrazine is toxic by vapor inhalation and skin absorption.)** Electric-field directed assembly was carried out in an MBraun nitrogen glovebox, and all solvents used were distilled and anhydrous.

Cyclic Voltammetry Measurements. Cyclic voltammograms were obtained employing a three-electrode C3 cell stand and Epsilon electrochemical workstation (Bioanalytical Systems, Inc.). 0.1 M tetrabutylammonium hexafluorophosphate (TBAPF$_6$) was used as the supporting electrolyte in acetonitrile. A platinum disk and platinum wire were selected as working and counter electrodes, respectively. A Ag/AgNO$_3$ (nonaqueous) electrode was used as the reference electrode. The redox couple ferrocene/ferrocenium ion (Fc/Fc$^+$) provided an external standard. Each cycle was performed at a scan rate of 100 mV/s.

Blocking Layer. To achieve this structure, reversibly hydrazine treated and vacuum exposed NW FETs with predominantly *p*-type characteristics were used. All e-beam resists and developers were degassed and used inside an MBraun nitrogen glovebox. An e-beam resist bilayer of 495 PMMA A4 (MicroChem) and 950 PMMA A4 (Microposit) was spincast and baked under nitrogen at 180 °C for 2 min for each layer. The PMMA coated device was secured in a jar under nitrogen in the glovebox and taken to the e-beam lithography tool, where the blocking layer was exposed. After exposure, the sample was developed in the glovebox with methyl isobutyl ketone in isopropyl alcohol (MIBK:IPA 1:3, Honeywell Burdick and

Jackson). E-beam evaporation of the 50 nm SiO_2 blocking layer was carried out in a nitrogen glovebox with an integrated evaporator, followed by lift-off with anhydrous acetone.

An Agilent 4156C parameter analyzer in combination with a Karl Suss PM5 probe station mounted in the nitrogen glovebox was used to measure device characteristics. The source was grounded, and a highly *n*-doped silicon wafer was used as a back gate electrode.

Supporting Information Available: Characterization of PbSe NWs, as well as electric-field assisted alignment of PbSe NW FETs and fabrication of the blocking layer. This material is available free of charge via the Internet at http://pubs.acs.org.

REFERENCES AND NOTES

1. Talapin, D. V.; Murray, C. B. PbSe Nanocrystal Solids for n- and p-Channel Thin Film Field-Effect Transistors. *Science* **2005,** *310*, 86–89.
2. Hang, Q.; Wang, F.; Carpenter, P. D.; Zemlyanov, D.; Zakharov, D.; Stach, E. A.; Buhro, W. E.; Janes, D. B. Role of Molecular Surface Passivation in Electrical Transport Properties of InAs Nanowires. *Nano Lett.* **2008,** *8*, 49–55.
3. Ko, D.; Urban, J. J.; Murray, C. B. Carrier Distribution and Dynamics of Nanocrystal Solids Doped with Artificial Atoms. *Nano Lett.* **2010,** *10*, 1842–1847.
4. Liang, W. J.; Hochbaum, A. I.; Fardy, M.; Rabin, O.; Zhang, M. J.; Yang, P. D. Field-Effect Modulation of Seebeck Coefficient in Single PbSe Nanowires. *Nano Lett.* **2009,** *9*, 1689–1693.
5. Zhao, N.; Osedach, T. P.; Chang, L. Y.; Geyer, S. M.; Wanger, D.; Binda, M. T.; Arango, A. C.; Bawendi, M. G.; Bulovic, V. Colloidal PbS Quantum Dot Solar Cells with High Fill Factor. *ACS Nano* **2010,** *4*, 3743–3752.
6. Yu, Y.; Kamat, P. V.; Kuno, M. A CdSe Nanowire/Quantum Dot Hybrid Architecture for Improving Solar Cell Performance. *Adv. Funct. Mater.* **2010,** *20*, 1464–1472.
7. Jarosz, M. V.; Porter, V. J.; Fisher, B. R.; Kastner, M. A.; Bawendi, M. G. Photoconductivity Studies of Treated CdSe Quantum Dot Films Exhibiting Increased Exciton Ionization Efficiency. *Phys. Rev. B* 2004, *70*, 195327.
8. Wise, F. W. Lead Salt Quantum Dots: The Limit of Strong Quantum Confinement. *Acc. Chem. Res.* **2000,** *33*, 773–780.
9. Yu, D.; Wang, C. J.; Guyot-Sionnest, P. n-Type Conducting CdSe Nanocrystal Solids. *Science* **2003,** *300*, 1277–1280.
10. Law, M.; Luther, J. M.; Song, O.; Hughes, B. K.; Perkins, C. L.; Nozik, A. J. Structural, Optical, and Electrical Properties of PbSe Nanocrystal Solids Treated Thermally or with Simple Amines. *J. Am. Chem. Soc.* **2008,** *130*, 5974–5985.
11. Norris, D. J.; Efros, A. L.; Erwin, S. C. Doped Nanocrystals. *Science* **2008,** *319*, 1776–1779.
12. Talapin, D. V.; Black, C. T.; Kagan, C. R.; Shevchenko, E. V.; Afzali, A.; Murray, C. B. Alignment, Electronic Properties, Doping, and On-Chip Growth of Colloidal PbSe Nanowires. *J. Phys. Chem. C* **2007,** *111*, 13244–13249.
13. Murphy, J. E.; Beard, M. C.; Nozik, A. J. Time-Resolved Photoconductivity of PbSe Nanocrystal Arrays. *J. Phys. Chem. B* **2006,** *110*, 25455–25461.
14. Luther, J. M.; Law, M.; Song, Q.; Perkins, C. L.; Beard, M. C.; Nozik, A. J. Structural, Optical and Electrical Properties of Self-Assembled Films of PbSe Nanocrystals Treated with 1,2-Ethanedithiol. *ACS Nano* **2008,** *2*, 271–280.
15. Tisdale, W. A.; Williams, K. J.; Timp, B. A.; Norris, D. J.; Aydil, E. S.; Zhu, X. Y. Hot-Electron Transfer from Semiconductor Nanocrystals. *Science* **2010,** *328*, 1543–1547.
16. Cho, K. S.; Talapin, D. V.; Gaschler, W.; Murray, C. B. Designing PbSe Nanowires and Nanorings Through Oriented Attachment of Nanoparticles. *J. Am. Chem. Soc.* **2005,** *127*, 7140–7147.
17. Sykora, M.; Koposov, A. Y.; McGuire, J. A.; Schulze, R. K.; Tretiak, O.; Pietryga, J. M.; Klimov, V. I. Effect of Air Exposure on Surface Properties, Electronic Structure, and Carrier Relaxation in PbSe Nanocrystals. *ACS Nano* **2010,** *4*, 2021–2034.
18. Leschkies, K. S.; Kang, M. S.; Aydil, E. S.; Norris, D. J. Influence of Atmospheric Gases on the Electrical Properties of PbSe Quantum-Dot Films. *J. Phys. Chem. C* **2010,** *114*, 9988–9996.
19. Dai, Q. Q.; Wang, Y. N.; Zhang, Y.; Li, X. B.; Li, R. W.; Zou, B.; Seo, J.; Wang, Y. D.; Liu, M. H.; Yu, W. W. Stability Study of PbSe Semiconductor Nanocrystals over Concentration, Size, Atmosphere, and Light Exposure. *Langmuir* **2009,** *25*, 12320–12324.
20. Sze, S. M.; Kwok, K. *Physics of Semiconductor Devices*, 3rd ed.; John Wiley & Sons: Hoboken, NJ, 2007.
21. Rogacheva, E. I.; Tavrina, T. V.; Grigorov, S. N.; Nashchenkina, O. N.; Volobuev, V. V.; Fedorov, A. G.; Nasedkin, K. A.; Dresselhaus, M. S. Effect of Oxidation on the Thermoelectric Properties of PbSe Thin Films. *J. Electron. Mater.* **2002,** *31*, 298–303.
22. Rogacheva, E. I; Tavrina, T. V.; Nashchekina, O. N.; Grigorov, S. N.; Sipatov, A. Y.; Volobuev, V. V.; Dresselhaus, M. S.; Dresselhaus, G. Influence of Oxidation on the Transport Properties of IV-VI-Thin Films. *Physica E* **2003,** *17*, 310–312.
23. Gottfried, J. M.; Elghobashi, N.; Schroeder, S. L. M.; Christmann, K. Oxidation of Gold by Oxygen-Ion Sputtering. *Surf. Sci.* **2003,** *523*, 89–102.
24. Ron, H.; Matlis, S.; Rubinstein, I. Self-Assembled Monolayers on Oxidized Metals. 2. Gold Surface Oxidative Pretreatment, Monolayer Properties, and Depression Formation. *Langmuir* **1998,** *14*, 1116–1121.
25. He, Y. J.; Wu, W. P.; Zhao, G. J.; Liu, Y. Q.; Li, Y. F. Poly(3,6-dihexyl-thieno[3,2-b]thiophene vinylene): Synthesis, Field-Effect Transistors, and Photovoltaic Properties. *Macromolecules* **2008,** *41*, 9760–9766.
26. Wan, A.; Hwang, J.; Amy, F.; Kahn, A. Impact of Electrode Contamination on the α-NPD/Au Hole Injection Barrier. *Org. Electron.* **2005,** *6*, 47–54.
27. Shpaisman, H.; Har-Lavan, R.; Stein, N.; Yaffe, O.; Korobko, R.; Seitz, O.; Vilan, A.; Cahen, D. Electronic Contact Deposition onto Organic Molecular Monolayers: Can We Detect Metal Penetration? *Adv. Funct. Mater.* **2010,** *20*, 2181–2188.
28. Chen, J.; Klinke, C.; Afzali, A.; Avouris, P. Self-Aligned Carbon Nanotube Transistors with Charge Transfer Doping. *Appl. Phys. Lett.* **2005,** *86*, 123108.
29. Klinke, C.; Chen, J.; Afzali, A.; Avouris, P. Charge Transfer Induced Polarity Switching in Carbon Nanotube Transistors. *Nano Lett.* **2005,** *5*, 555–558.
30. Tung, V. C.; Allen, M. J.; Yang, Y.; Kaner, R. B. High-Throughput Solution Processing of Large-Scale Graphene. *Nat. Nano.* **2009,** *4*, 25–29.
31. Timp, B. A.; Zhu, X. Y. Electronic Energy Alignment at the PbSe Quantum Dots/ZnO(1010) Interface. *Surf. Sci.* **2010,** *604*, 1335–1341.
32. Kovalenko, M. V.; Scheele, M.; Talapin, D. V. Colloidal Nanocrystals with Molecular Metal Chalcogenide Surface Ligands. *Science* **2009,** *324*, 1417–1420.
33. Mitzi, D. B.; Kosbar, L. L.; Murray, C. E.; Copel, M.; Afzali, A. High-Mobility Ultrathin Semiconducting Films Prepared by Spin Coating. *Nature* **2004,** *428*, 299–303.